



Design and Simulation of a Crash Energy Absorption System Integrated with Magneto-Rheological Absorber

Pavan Kumar Archakam¹ · Sreekumar Muthuswamy¹

Received: 2 December 2020 / Revised: 5 April 2021 / Accepted: 8 May 2021 / Published online: 2 June 2021
© Krishtel eMaging Solutions Private Limited 2021, corrected publication 2021

Abstract

Purpose The global car crash fatalities are mostly due to the frontal collisions. The head-on collision of a car leads to the dangerous intrusion of the bumper and other frontal parts of the vehicle towards the passenger compartment. The frontal structure needs to have a proper adaptable crash energy absorption system to reduce the intrusion. A new crash energy absorption system combined with a Magneto-Rheological Absorber (MRA) has been proposed to meet the above requirements.

Methods The design and modeling of the system based on magneto-rheological (MR) technology generally comprise of mathematical formulation, numerical simulation, and validation with a physical test. The current work focuses on lumped parameter modeling (LPM) of a light passenger car equipped with MRA in serial and parallel configurations. The modified Bouc–Wen model has been used in the design of MRA as it is the most standard form to model non-linear hysteretic systems. In this work, six new models are proposed by varying the position of MRA in the standard one degree of freedom (DoF) Kelvin–Voigt model and two-DoF model. The performance of the proposed models has been simulated in MATLAB–SIMULINK environment, considering various initial velocities of the vehicle by supplying different voltages to MRA.

Results The results show that three of the six proposed models exhibit better crash kinematic responses than the base models, which are experimentally validated and available in existing literature. Finally, the MRA behavior has been captured to validate its effectiveness in the design of the crash energy absorption system. The proposed methods are also useful in the development of crash mitigation devices in electric vehicles (EVs). The results obtained would be utilized in design of a multi-stage crash energy absorption system.

Conclusion Thus, the collision energy absorption system with add-on MRAs behaves as a semi-active system. It is efficient during various high-speed impacts and can be implemented practically. The proposed methods are also useful in the development of crash mitigation devices in electric vehicles (EVs).

Keywords Magneto-Rheological Absorber (MRA) · Modified Bouc–Wen model · Kelvin–Voight model · Crash energy absorption · Numerical simulation

Introduction

According to the World Health Organization (WHO), approximately 10% of total road crash fatalities were happening in India compared to all other parts of the Globe, including the highest populous country, China [1]. The report of the National Crime Records Bureau (NCRB) of

India reveals that there is a dangerous increment in the fatality rate up to 44.2% during the decade, 2001–2011, which shows that there was one death for every five minutes on Indian roads. If this trend continues up to 2020, there would be a drastic change, and it can reach three casualties for every 5 min. Among these road accidents, car crash amounts to a significant fraction of the total fatalities. The fatalities are mostly due to the transmission of impact energy in the form of vibration in the interior of the vehicle during the collision. According to the “British Motor Insurance Repair Research Centre” study on vehicle damage for different configuration of collisions, 65% of vehicles were damaged due to front impacts, 25% due to the rear effects, 5% each due to the left- and right-side collision [2].

✉ Sreekumar Muthuswamy
msk@iiitdm.ac.in

¹ Centre for AI, IoT, and Robotics, Department of Mechanical Engineering, Indian Institute of Information Technology, Design and Manufacturing, Kancheepuram, Chennai 600127, India

Most of the designs were concentrated on frontal collisions to reduce the impact force transmitted to the occupant's cabin. Although there are many passive safety systems to rescue the occupants such as seat belts, crumple zones, and airbags, still there is a need for an active and controllable frontal structure for automobiles, especially for passenger cars. The proposed crash energy absorption system is an adaptable semi-active system integrated with MRA and located behind the bumper.

The vehicle crash scenario can be modeled in various ways,

including lumped parameter modeling, finite element modeling, multibody dynamic modeling, and hybrid modeling. The present work focuses on LPM because of its ease of operation and capability to offer the closest outputs compared with real-time crash tests [3]. The simple one-DoF model also called a Kelvin–Voigt model [4], is extensively used in the development of the proposed system. Kamal et al. [5] proposed three DoF-lumped parameter models of the frontal collision: eight frontal elastic parts (torque box, front frame, driveline, sheet metal, firewall, radiator setup, engine mounts, and transmission mounts) were modeled as linear spring elements. The body chassis mass, engine transmission mass, and engine cross member mass were modeled as lumped masses.

MR fluids, invented long back in the late 1940s by Jacob Rabinow [6] at the US National Bureau of Standards, are finding broad applications because of their excellent features such as low viscosity and high yield strength. The MR fluids [7] are developed by mixing appropriate magnetizable particles (1–10 μm) suspended in a carrier fluid such as mineral oil or synthetic oil. Carbonyl iron particles are generally used as magnetizable particles in the ratio of 20%–40% by volume. Ahmed et al. [8] reviewed several types of MR materials, their modeling, existing devices and their applications in various fields. Various metal foam-based MR fluid materials were formed, and experimental investigations had been carried out for the validation of dynamic response with finite element simulation [9]. Shear performance of metal foam Nickel-based MR fluid damper [10] was tested by constructing a test rig, and results were compared with magnetic field simulations in ANSYS. The authors have concluded that the damping force is decreasing with an increase in shear rate.

MRA's structural advancements are broadly categorized as three elemental improvements [11] such as coil number and distribution, magnetic circuit, and damping channel. Advanced modeling, design techniques with optimized geometry, construction, and classification of MR fluid damper had already been discussed Rahman et al. [12]. MRA is a semi-active device which comprises of damper housing, piston with a shaft, MR fluid, and gas chamber, as shown in Fig. 1a. The piston moves inside the damper

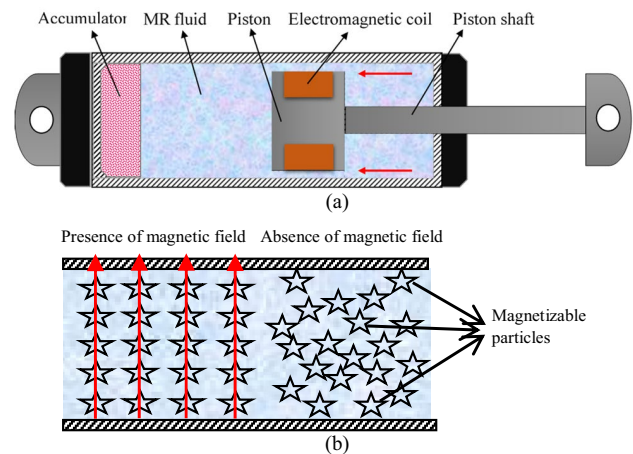


Fig. 1 MRA. a Parts. b Working principle

housing with a small gap between piston and housing for the MR fluid to flow. Inside the piston, an electromagnetic coil is placed in such a way that the induced magnetic field can flow through the MR fluid. This magnetic field intensity changes the MR fluid's viscosity by the alignment of magnetic particles along the field lines, as shown in Fig. 1b. Thus, the force required to actuate the piston is directly proportional to the viscosity of the MR fluid. As the current supplied increases, the magnetic field induced in the coil also increases. In addition, the suspended magnetic particles align along the magnetic field lines, and this makes the MR fluid to behave like a semi-solid. Finally, a greater force is required to move the piston, as its yield stress varies in response to the applied magnetic field.

The development of magnetic field plays a vital role in the damper performance. There are two terms such as magnetic field strength (H) and magnetic flux density (B) and their relation, i.e., the B – H curve needs to be considered as the property of the MR fluid. For the present work, the prototype damper developed by Spencer [13] having magnetic field strength varying from 0 to 200 KA/m for 0–1A current flow inside the coil is considered.

Hence, the damping force can be varied by controlling the current in the coil based on the external shock. These dampers can be operated in a squeeze, shear, and valve modes. In this work, valve mode is used to force the fluid in between two reservoirs in the presence of a magnetic field.

The recent development in MR technology has been proven in many applications like the semi-active suspension system [14], MR clutches, brakes in automobiles, and vibration mitigation devices for seismic protection of structures [15], and in several bio-engineering applications as well. The existing proposed dynamic models of MR devices based on constitutive mechanical models and their control strategies for various applications had been systematically

reviewed in [16] Yingkun et al. [17] proposed a hybrid frame of the vehicle by combining MR dampers for lateral vibration mitigation, which are modeled with Bouc–Wen-based Support-Vector Machine (SVM) model. The authors also validated the dynamic characteristics of a hybrid frame with sinusoidal and random excitations by comparing simulation results in ANSYS using test data. The application of MRAs in vehicle suspension has been increased because of its advanced features in shock absorption during the locomotion of the vehicle. Guoliang et al. [18] proposed a novel MR damper with self-sensing displacement and vibration energy harvesting capability and also evaluated its performance by conducting FEA simulation with experimental validation. Although MR dampers are extensively used for the structural vibration mitigation and vehicle suspension, very few researchers have studied the application of MRA in crash energy absorption of automobiles, which requires high damping force. To improve the damping force capability up to 3400 N with an excitation velocity 0.0625 m/s, Cheng et al. [19] presented a theoretical model of a meandering magnetic circuit MR damper and performed the finite element analysis to validate the experimental results.

A study by Ahmadian et al. [20] presented an experimental evaluation of MR damper based on impact and shock loading by performing a drop tower test. In this evaluation, various impact velocities were achieved by varying heights and drop-masses. An experimental setup for impact absorber was fabricated as a drop-pendulum test-rig, and a vehicle model with MRA was developed by Pokaaad et al. [21]. A polynomial model of MR impact absorber was proposed in [22], and parameters such as deceleration, acceleration, and fluid locking regions were compared with the physical model for three categories of vehicles such as a common vehicle, a vehicle with a passive bumper, and a vehicle with controlled bumper based on the sky-hook system. Dong et al. [23] performed a numerical simulation using the human simulated slide mode controller in the vehicle collision absorption system with two-DoF lumped parameter model. The Bingham model was considered by the authors for the MRA to validate MR collision absorption. Ahmed et al. [24] suggested an idea of arranging MR damper and spring in series in front of the vehicle overhung and also proposed a theoretical model of it.

Bai et al. [25] proposed an inner bypass MR damper for ground vehicle suspensions with five electromagnetic coils. These can simultaneously enhance dynamic range (ratio of on-state to off-state damping force) and minimizes off-state load at high piston velocities. The nonlinear Bingham-Plastic fluid model was used as a theoretical model and validated with test results obtained from a prototype damper. Lingyu et al. [26] proposed a magnetorheological elastomer-based energy absorption device (MREBEAD) installed behind the vehicle bumper to give flexibility based on the nature of

collision. It is more effective than the crash box and also reduces the cost of repair and injury in low-speed collisions. Woo et al. [27] suggested that the frontal crash mitigation is possible by the development of a controllable bumper using MR impact damper and proposed the dynamic modeling of three-DoF vehicle model combined with two-DoF occupant model. The research outcomes confirmed the good damping capability of MR dampers during a frontal collision using the vehicle crash severity index (VCSI) as a performance criterion. Wang et al. [28] presented a dynamic simulation of MR damper under impact loads in MATLAB–SIMULINK and validated the simulation results with an experimental test rig. Arsava et al. [29] proposed nonlinear models of MR dampers for a variety of impact loads and compared them with Bingham and Bouc–Wen models.

Some researchers had earlier suggested the development of dynamic modeling of smart systems by add-on hydraulic absorbers. Also, they have compared the collision situations of both smart structured vehicle and standard vehicle with deformation, deceleration responses for the vehicle to vehicle and vehicle to moving barrier collision [30]. Jawad [31] proposed an extendable hydraulic smart structure within the longitudinal member that could modify stiffness according to the severity of the frontal collision. The Baja vehicle's frontal and rear frames were attached with the shock absorbers to suppress the impact load during the head-on and rear collision. Also, the authors have performed a transient dynamic analysis in ANSYS Workbench for various contact conditions [32]. Elmarakbi et al. [33] proposed two types of smart frontend systems, which are fixed and extendable structures. An analytical approach called incremental harmonic balance method (IHBM) was intended to enhance the crashworthiness of frontal structure during full and offset collisions. The pneumatic energy absorption system has been proposed in [34], which can elongate or compress the energy absorption beam automatically as per the collision. The conceptual design of a novel 4-stage collision energy absorbing system, which comprises of the bumper, MRA, spring with piston cylinder, and the shear plate was proposed in [35]. Also, steps for modeling of MRA were suggested. Still, there is a scope for the development of the MR collision absorption system as per the crash severity. An attempt has been made in the present work to address the vehicle's behavior during collision using LPM by changing the position of MRA.

The features of the work presented and the comparison with existing literature are shown in Table 1. Non-linear behavior of the vehicle during a frontal collision by combining MRA in parallel, and series configurations are yet to be studied in detail. The proposed non-linear dynamic models are new, complex, and developed by arranging MRA in various configurations within the vehicle's frontal structure. The collision models have been derived based on LPM. The

Table 1 Highlights of the proposed research compared to existing literature

Sl.N	Description	Existing work	Present proposed work
1	Model of MRA	Bingham model [23] Hydraulic model [24, 27] Non-parametric-polynomial model [21]	Parametric based modified Bouc–Wen model has been considered from [13]
2	Nature of modelling	Linear [23, 27]	Considered as non-linear hysteretic system
3	Vehicle model	LPM [23] LPM compared with prototype vehicle [27]	LPM parameters have been selected based on crash testing of a real-time vehicle from [4, 41]
4	Configuration of MRA	Single configuration next to bumper [21, 23, 24, 27]	Various configurations such as parallel and series combinations with one- and two-DoF crash models
5	Dampers	Hydraulic dampers (passive) [32] Pneumatic energy absorption structure [34]	Semi-active devices, i.e., MRAs have been used
6	Theoretical models	MR dampers in front overhung for four-wheeler as impact reducing systems [24] Four stage collision energy absorption system [35] a magnetorheological elastomer (MRE)-based adaptive energy absorption device (MREBEAD) [26] Hydraulic smart structure without mRA [30] [31] [33]	Dynamic modelling and numerical simulation of semi-active smart crash energy absorption system with MRA in various combinations with the frontal structure of the vehicle The behavior of MRA has been captured for various impact velocities and voltages

existing non-linear hysteresis parametric model, named as modified Bouc–Wen model proposed by spencer [13], has been utilized for MRA.

Although MRA has been modeled as per the existing literature, the present work is related to the integration of MRA in the frontal structure of the vehicle in different configurations. This aspect is unique and not available in the literature. As far as the knowledge of the authors, few literature are related to the current manuscript. The information available is limited in the development of the crash energy absorption system for the following reasons.

- The MRA had been modeled as the Bingham model, which is linear.
- The MRA is integrated with the vehicle next to the bumper in series combination only.
- Real-time optimized parameters were not utilized in the prototype vehicle that had been used for testing.

The current scenario of the world is moving towards EVs by transforming the internal combustion (IC) engine into electrical motor and batteries. There are two types of conversions: one is fully replacing the IC engine into a battery-powered one, and the other is a hybrid vehicle developed by replacing the large IC engine with a small IC engine and an electrical motor with battery. In the present context of a frontal crash, IC engine vehicle has frontal parts such as the bumper, crush box, radiator, engine, etc. that act as a crushable zone; whereas for EVs, there is no requirement of these frontal parts. Xiao et al. [36] proposed an alternative approach by designing and optimizing the flexible battery packs as a crash absorbing structure of the EVs during

frontal collisions. The limitation of this approach is with the maximum probability of catching fire in the battery packs due to the development of high friction during a collision. Hence, some standard structure needs to be developed for the absorption of crash energy. The proposed system will also help develop crash-proof structures for EVs by incorporating MRAs in front of the vehicle. The peak power consumed by MRA is approximately less than 10 W, which would be expected to function continuously for more than an hour [13].

The present proposed work deals with the numerical study of the crash energy absorption system for the low-speed impact, such as frontal localized pole collision, with MRA as add-on energy absorbing element. An LPM has been established to formulate dynamic equations for various assembled positions of MRA with one-DoF and two-DoF crash systems. The parameters such as stiffness, damping coefficient, and lumped mass were extracted from literature, which were already validated with the experimental test results. These parameters help to compare the base models and the proposed models (equipped with MRA). The numerical study is performed in MATLAB/SIMULINK environment with a focus on crash pulse analysis to emphasize the crash energy absorbing capability of the system and the associated behavior of MRA during a crash with various impact velocities.

The paper has been organized as follows. The mathematical modeling of MRA with hysteretic effect and details on numerical simulation for plotting the characteristic curves are discussed in Sect. 2 for the validation of the MRA's Simulink model. Section 3 gives information regarding the existing base models of one- and two-DoF systems. Dynamic

equations, details on the selection of parameters that have been validated with existing literature are also described in Sect. 3. Section 4 explains the physical and mathematical modeling of the proposed lumped parameter models incorporated with MRAs. In Sect. 5, the results obtained from numerical simulation of the base models and the proposed models have been discussed in detail. Then conclusions are drawn, followed by references.

Mathematical Modeling of MRA

MRAs are generally used in semi-active suspension systems to mitigate vibrations coming from the uneven road. The models available in the existing literature are classified as parametric models [37, 38] and non-parametric models [39, 40]. The various parametric models are Bingham-model-based dynamic, viscoelastic–plastic, Bouc–wen, and modified Bouc–wen models with hysteresis, biviscous, stiffness–viscosity elasto-slide, Dahl hysteresis operator-based, hyperbolic tangent function-based, LuGre hysteresis operator-based, and Sigmoid function-based models. There are non-parametric models that also have good capability to capture behavior of MRA such as polynomial, black-box, neural network, fuzzy, multifunction, wavelets, fuzzy neural network, query-based models, ridgenet mode neural networks, and particle swarm optimization.

The non-parametric models are more accurate than parametric. The present work is based on LPM, which requires parametric, i.e., mechanical model (spring mass damper system) of MRA to integrate it into the vehicle. The models such as Bingham, Gamota and Filisko, Bouc–Wen, Dahl, LuGre, and modified Bouc–Wen models, etc. are known as mechanical models [41]. Amongst these models, the modified Bouc–Wen model with hysteresis is versatile and the frequently used model in literature [42, 43] for various applications of non-linear hysteretic systems. This model is exhibiting close approximation with experimental results for various input excitations, as demonstrated by Spencer [13]. Even though this model was proposed in 1997, many recent research works have been carried out with this model for various applications. Hence, the utilization of the modified Bouc–Wen model in the present work is justified.

The lumped parameter model of the MRA is shown in Fig. 2. The springs and dampers are arranged in parallel by considering the effect of hysteresis to incorporate the non-linearity effect of the system. When an external excitation is applied on the damper, either to elongate or to compress the system, a resistance force of the same magnitude would be generated. This force is called as the damping force, and it always acts in the opposite direction of the applied force.

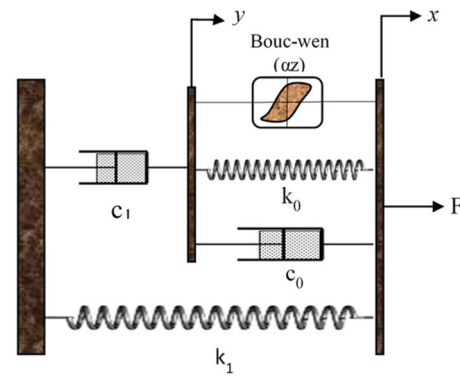


Fig. 2 Modified Bouc–Wen model for MRA

The following are the seven governing dynamic equations of MRA, as presented in [13]; however, they are reproduced below considering their importance in this work.

$$F = c_1 \dot{y} + k_1(x - x_0), \quad (1)$$

$$\dot{y} = \frac{1}{c_0 + c_1}(\alpha z + c_0 \dot{x} + k_0(x - y)), \quad (2)$$

$$\dot{z} = \begin{cases} -\gamma z |\dot{x} - \dot{y}| |z|^{n-1} - \beta(\dot{x} - \dot{y}) |z|^n \\ + A(\dot{x} - \dot{y}) \end{cases}, \quad (3)$$

$$\alpha = \alpha(u) = \alpha_a + \alpha_b u, \quad (4)$$

$$c_0 = c_{0a} + c_{0b} u, \quad (5)$$

$$c_1 = c_{1a} + c_{1b} u, \quad (6)$$

$$\dot{u} = -\eta(u - v), \quad (7)$$

where F -damping force, c_1 - viscous damping coefficient at low velocities, k_1 - accumulator stiffness, c_0 -viscous damping coefficient at high velocities, α - evolutionary coefficient, k_0 -control stiffness at high velocities, x_0 - initial displacement of spring k_1 associated with the nominal damper force due to the accumulator. The displacement of input excitation, displacement of the piston, and the hysteretic component of MRA are represented as x , y , and z , respectively. γ , β , and A are hysteresis parameters of yield element. The parameters related to (4)–(6) are dependent on filtered voltage u . The first-order filter in (7) shows the relation between filtered voltage u and applied voltage v . These parameters related to a generalized model are shown in Table 2.

Table 2 Parameters considered for the generalized model of MRA [13]

Sl. no	Parameter	Value	Sl. No	Parameter	Value
1	c_{0a}	2100 Ns/m	8	k_0	4690 N/m
2	c_{0b}	350 Ns/mV	9	k_1	500 N/m
3	c_{1a}	28,300 Ns/m	10	x_0	0.143 m
4	c_{1b}	295 Ns/mV	11	γ	$363 \times 10^4 \text{ m}^{-2}$
5	α_a	14,000 N/m	12	β	$363 \times 10^4 \text{ m}^{-2}$
6	α_b	69,500 N/mV	13	A	301
7	η	190 s^{-1}	14	n	2

Numerical Simulation

The MRA is modeled in MATLAB–SIMULINK by incorporating all the seven governing equations from (1) to (7). The numerical analysis is performed to validate the SIMULINK model developed using the data available in Table 2. In the present simulation, MRA is considered to be operated at a resistance of 3Ω , with the amplitude of sinusoidal excitation as 1.5 cm and frequency 2.5 Hz for various voltage inputs, ranging from 0 to 2.5 V as shown in Fig. 3.

The characteristic responses, such as damping force vs time, force vs displacement, and force vs velocity, are shown in Fig. 4. Similar results were already presented in [13]; however, verified again as the MRA is integrated with the proposed system. From these results, it can be observed that the damping force as a function of time increases with an increase in applied voltage, as seen in Fig. 4a. The force–displacement response (Fig. 4b) is approximately elliptical along a clockwise path. Figure 4c depicts force–velocity response, which forms almost linearly varying hysteresis loop as per the applied voltage and progress along an anti-clockwise path. The characteristics of MRA are closely matching with the experimental tests, as presented in [13]. Hence, the SIMULINK block model is validated and used in the present numerical analysis as well.

Proposed Methodology, Base Models of Vehicle and Selection of Parameters

The present proposed original methodology is shown in Fig. 5, which depicts the LPM of the collision energy absorption system by combining MRA in series and parallel configurations with one-DoF and two-DoF base models.

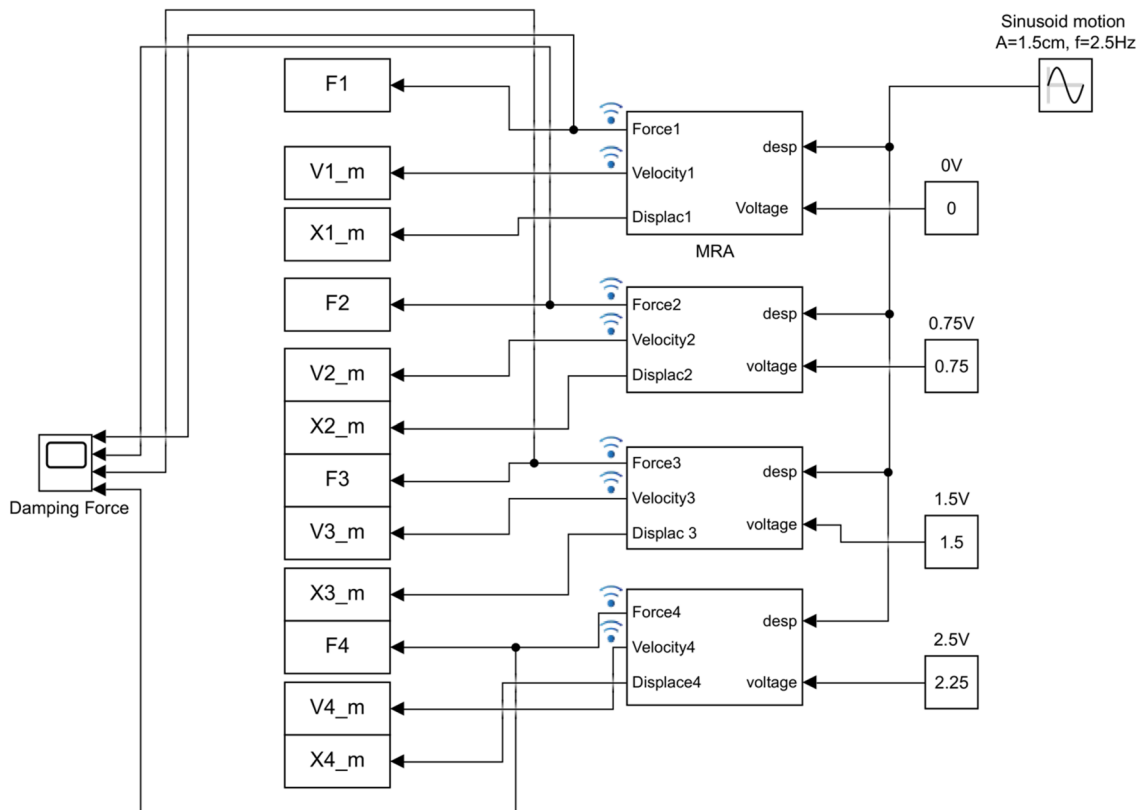


Fig. 3 Simulink model of MRA for various voltages

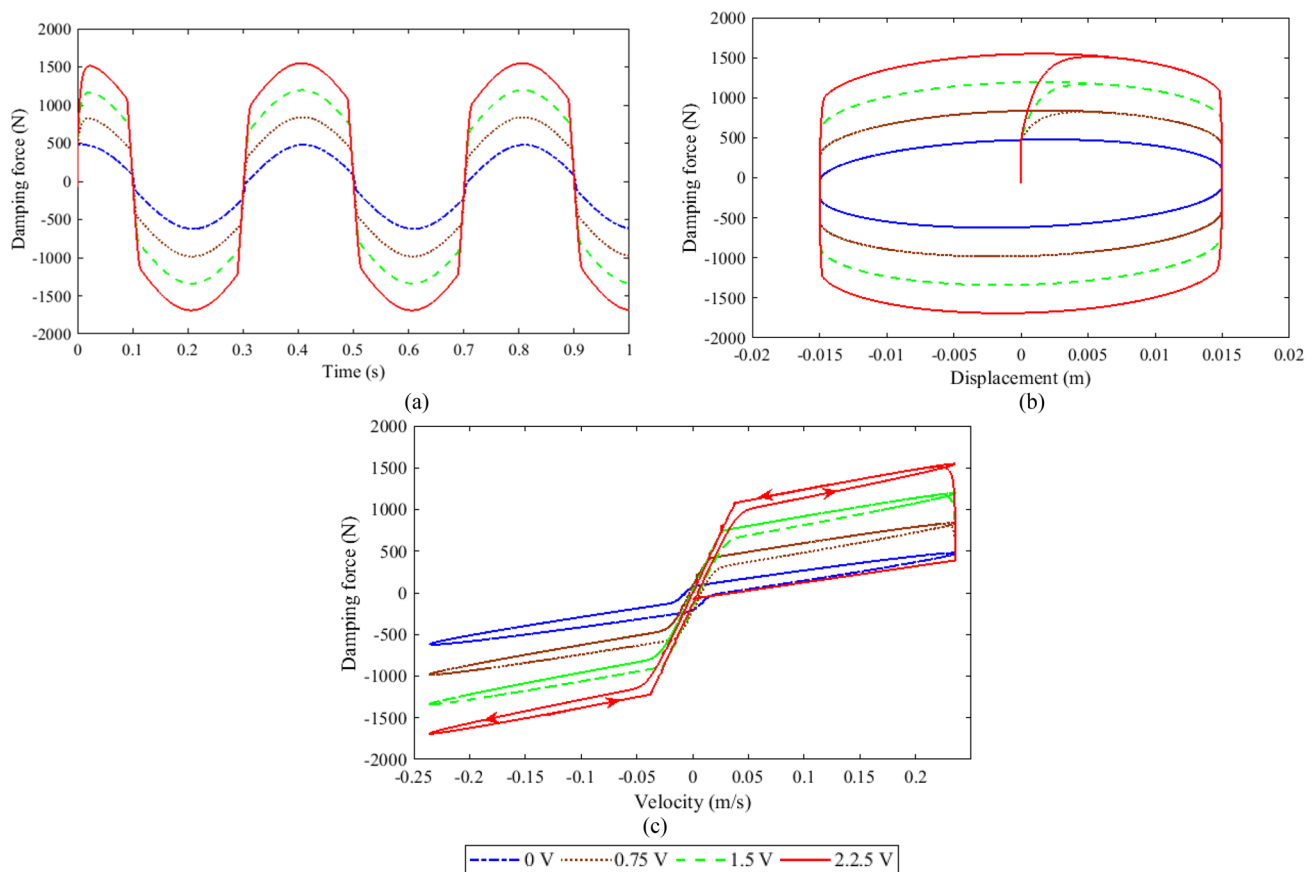


Fig. 4 The response of MRA. **a** Force vs time. **b** Force vs displacement. **c** Force vs velocity

The complex dynamic equations have been derived and modeled in a block diagram-based programming language called MATLAB–SIMULINK. The quantitative evaluation has been performed by comparing base and proposed models of one-DoF and two-DoF models individually. The results are categorized as crash kinematics, characteristics of MRA for various voltages and velocities.

The real-time vehicle crash can be formulated by the lumped parameter model. This model offers almost similar results compared to the available experimental data. The lumped parameter models are designed with discrete masses concentrated on a certain point. Primarily, the car is modeled as a single-DoF model (Kelvin–Voigt model) with linear spring, linear-viscous damper, and single lumped mass. The kinematic responses of mass are denoted as x , \dot{x} , \ddot{x} , and the physical model is shown in serial number 1 of Table 3. The same vehicle can also be modeled as a two-DoF model for more accuracy, which contains frontal parts, engine mass as one concentrated mass M_1 , and occupant's cabin mass as another concentrated mass M_2 . The kinematic responses of mass M_1 and M_2 are represented as x_1 , \dot{x}_1 , \ddot{x}_1 , and x_2 , \dot{x}_2 , \ddot{x}_2 , respectively. The associated physical model is shown in

serial number 2 of Table 3. These are the two base models considered to integrate the MRA in the crash energy absorption system.

The governing equations are derived with the help of Newton's second law of motion by constructing free-body diagrams (8)–(9).

The selection of parameters is a critical part of the numerical simulation. The parameters for one-DoF model are considered according to the kinematic responses of the vehicle obtained from filtered data analysis [4] which are shown in Table 4. In the case of two-DoF model, the parameters selected from [44] are organized in Table 5.

Proposed Models by Incorporating MRA

Initially, the total vehicle is modeled as a one-DoF system by including two MRAs through parallel (integrated model) and series (extended model) combinations with the frontal structure of the vehicle. Their physical models are shown in serial numbers 1, 2 of Table 6. Later, the same vehicle is modeled as two-DoF models, and the MRAs are arranged in series

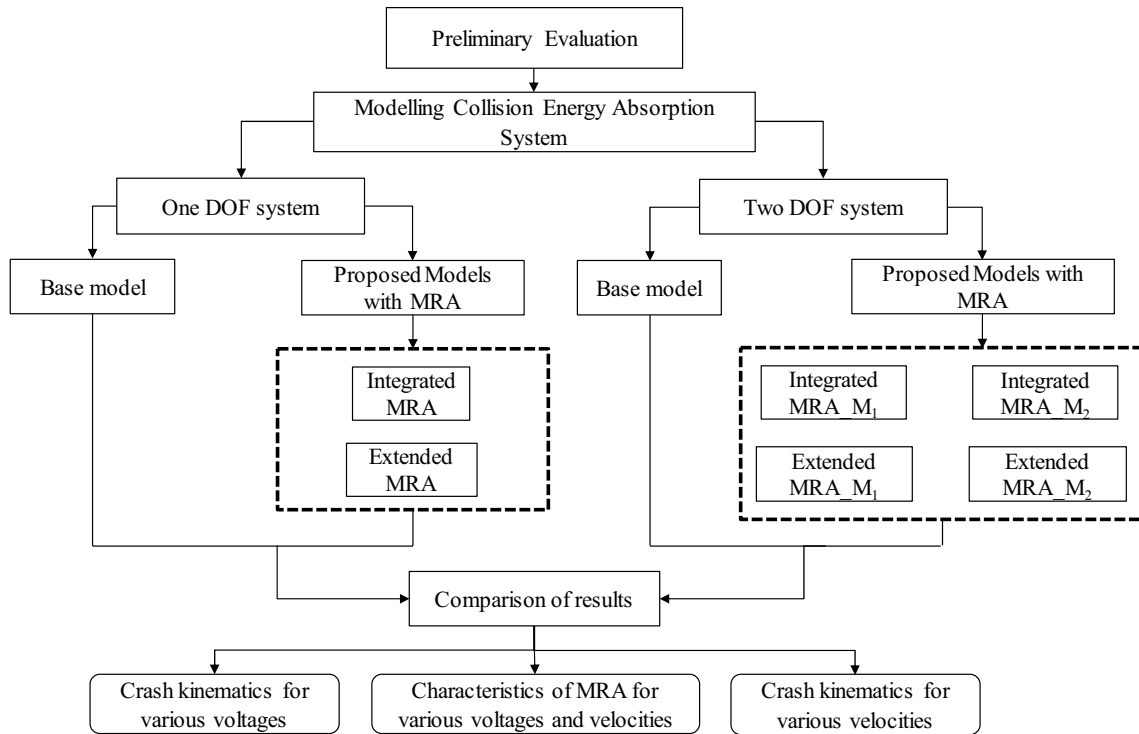
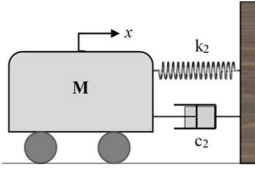
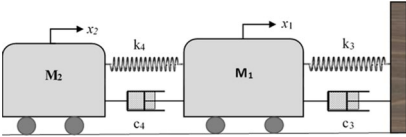


Fig. 5 The proposed methodology

Table 3 Base models of the vehicle

Sl. No	Model Name	Mathematical model	Eq. No	Physical model
1	One-DoF model	$M\ddot{x} + c_2\dot{x} + k_2x = 0$	(8)	
2	Two-DoF model	$M_1\ddot{x}_1 = -(k_3 + k_4)x_1 - (c_3 + c_4)\dot{x}_1 + k_4x_2 + c_4\dot{x}_2$ $M_2\ddot{x}_2 = c_4(\dot{x}_1 - \dot{x}_2) + k_4(x_1 - x_2)$	(9)	

and parallel combinations with lumped masses, which are mentioned as extended and integrated models, respectively, in the subsequent sections. Four such models are developed and shown in Table 6 (Sl. No. 3–6).

Table 4 Parameters for one-DoF model

Sl. No	Parameter	Value
1	M	873 kg
2	k_2	344,150 N/m
3	c_2	2427 Ns/m
4	v_i	35 km/h

Table 5 Parameters for two-DoF Model

Sl. No	Parameter	Value
1	M_1	582 kg
2	M_2	291 kg
3	k_3	74,681 N/m
4	k_4	45,821 N/m
5	c_3	18,176 Ns/m
6	c_4	11,196 Ns/m
7	v_i	35 km/h

Table 6 Various models proposed for crash absorption system incorporated with MRA

Sl. No	Model name	Mathematical model	Eq No	Physical model
1	One DoF integrated	$M\ddot{x} = \begin{cases} -2k_1(x-x_0) + k_2\dot{x} - 2k_0(x-y) - 2c_0(\dot{x}-\dot{y}) \\ -c_2\dot{x} - 2\alpha z \\ k_0(\dot{x}-\dot{y}) + c_0\dot{x} + \alpha z \\ (c_0 + c_1) \end{cases}$ $\dot{y} = \frac{k_0(\dot{x}-\dot{y}) + c_0\dot{x} + \alpha z}{(c_0 + c_1)}$ $\dot{z} = -\gamma \dot{x}-\dot{y} z z ^{n-1} - \beta(\dot{x}-\dot{y}) z ^n + A(\dot{x}-\dot{y})$ $F = c_1\dot{y} + k_1(x-x_0)$	(10)	
2	One DoF extended	$M\ddot{x} = -2k_0(x-y) - 2c_0(\dot{x}-\dot{y}) - 2k_1(x-x_s-x_0) - 2\alpha z$ $\dot{y} = \frac{c_1\dot{x}_0 + c_0\dot{x} + k_0(x-x-y) + \alpha z}{(c_0 + c_1)}$ $\dot{x}_0 = \frac{2c_1\dot{y} + 2k_1(x-x_s-x_0) + k_2x_0}{(2c_1 + c_2)}$ $\dot{z} = -\gamma \dot{x}-\dot{y} z z ^{n-1} - \beta \times (\dot{x}-\dot{y}) z ^n + A(\dot{x}-\dot{y})$ $F = c_1(\dot{y}-\dot{x}_0) + k_1(x-x_s-x_0)$	(11)	
3	Two DoF integrated with M1	$M_1\ddot{x}_1 = \begin{cases} -k_4(x_1-x_2) - c_4(\dot{x}_1-\dot{x}_2) - (2k_1+k_3)x_1 \\ -2c_0(\dot{x}_1-\dot{y}) - c_3\dot{x}_1 - 2k_0(x_1-y) - 2\alpha z \end{cases}$ $M_2\ddot{x}_2 = -k_4(x_2-x_1) - c_4(\dot{x}_2-\dot{x}_1) \\ c_0\dot{x}_1 + k_0(x_1-y) + \alpha z$ $\dot{y} = \frac{c_0\dot{x}_1 + k_0(x_1-y) + \alpha z}{c_0 + c_1}$ $\dot{z} = -\gamma \dot{x}_1-\dot{y} z z ^{n-1} - \beta \times (\dot{x}_1-\dot{y}) z ^n + A(\dot{x}_1-\dot{y})$ $F = c_1\dot{y} + k_1x_1$	(12)	
4	Two DoF extended with M1	$M_1\ddot{x}_1 = \begin{cases} -k_4(x_1-x_2) - c_4(\dot{x}_1-\dot{x}_2) - 2k_1(x_1-x_{s1}) \\ -2c_0(\dot{x}_1-\dot{y}) - 2k_0(x_1-y) - 2\alpha z \end{cases}$ $M_2\ddot{x}_2 = -k_4(x_2-x_1) - c_4(\dot{x}_2-\dot{x}_1) \\ c_0\dot{x}_{s1} + k_0(x_1-y) + c_0\dot{x}_1 + \alpha z$ $\dot{y} = \frac{c_0\dot{x}_1 + k_0(x_1-y) + c_0\dot{x}_1 + \alpha z}{c_0 + c_1}$ $\dot{x}_{s1} = \frac{2c_1\dot{y} + 2k_1(x_1-x_{s1}) - k_3x_{s1}}{(c_1 + c_3)}$ $\dot{z} = -\gamma \dot{x}_1-\dot{y} z z ^{n-1} - \beta(\dot{x}_1-\dot{y}) z ^n + A(\dot{x}_1-\dot{y})$ $F = c_1(\dot{y}-\dot{x}_{s1}) + k_1(x_1-x_{s1})$	(13)	

Table 6 (continued)

Sl. No	Model name	Mathematical model	Eq No	Physical model
5	Two DoF integrated with M_2	$M_1 \ddot{x}_1 = \left\{ \begin{array}{l} -(2k_1 + k_4)(x_1 - x_2) - c_4(\dot{x}_1 - \dot{x}_2) - k_3 x_1 \\ -2c_1(\dot{x}_1 - \dot{y}) - c_3 \dot{x}_1 \end{array} \right\}$ $M_2 \ddot{x}_2 = \left\{ \begin{array}{l} -(2k_1 + k_4)(x_2 - x_1) - c_4(\dot{x}_2 - \dot{x}_1) - 2k_0(x_2 - y) \\ -2c_0(\dot{x}_2 - \dot{y}) - 2\alpha z \end{array} \right\}$ $\dot{y} = \frac{c_0 \dot{x}_2 + c_1 \dot{x}_1 + k_0(x_2 - y) + \alpha z}{c_0 + c_1}$ $\dot{z} = -\gamma \dot{x}_2 - \dot{y} z ^{m-1} - \beta(\dot{x}_2 - \dot{y}) z ^n + A(x_2 - y)$ $F = c_1(\dot{y} - \dot{x}_1) + k_1(x_2 - x_1)$	(14)	
6	Two DoF extended with M_2	$M_1 \ddot{x}_1 = -k_4(x_1 - x_{s2}) - c_4(\dot{x}_1 - \dot{x}_{s2}) - k_3 x_1 - c_3 \dot{x}_1$ $M_2 \ddot{x}_2 = -2k_1(x_2 - x_{s2}) - 2k_0(x_2 - y) - 2c_0(\dot{x}_2 - \dot{y}) - 2\alpha z$ $\dot{y} = \frac{c_0 \dot{x}_2 + c_1 \dot{x}_{s2} + k_0(x_2 - y) + \alpha z}{c_1 + c_0}$ $\dot{x}_{s2} = \frac{c_4 \dot{x}_1 + 2c_1 \dot{y} + k_4(x_1 - x_{s2}) + 2k_1(x_2 - x_{s2})}{(2c_1 + c_4)}$ $\dot{z} = -\gamma \dot{x}_2 - \dot{y} z ^{m-1} - \beta(\dot{x}_2 - \dot{y}) z ^n + A(x_2 - y)$ $F = c_1(\dot{y} - \dot{x}_{s2}) + k_1(x_2 - x_{s2})$	(15)	

The MRA specified in sketches of Table 6 is considered based on the modified Bouc–Wen model, as discussed in Sect. 2. The dynamic Eqs. (10)–(15) are derived by blending the modified Bouc–Wen model with the vehicle model exploiting Newton’s second law of motion. The equations used to calculate the damping force (F) of MRA are also formulated and presented in this table. In the present work, the vehicle crash phenomenon is assumed to be a free damped vibration concept, as mentioned in [45] with input excitations such as initial velocity and displacement. For both the one-DoF and two-DoF models, deformation of the vehicle and occupant’s cabin is found to be of underdamped vibration with a sinusoidal response of exponentially decaying nature. The same reaction has been considered as input excitation to MRA. Hence, the utilization of the modified Bouc–Wen model for this type of response is appropriate and justified, as supported in the literature [13].

Bernard et al. [46] optimized the lumped parameters of the vehicle with an initial velocity of 56 km/h as per the experimental results available in the reports of National Highway Traffic Safety and Administration (NHTSA) for Ford-Taurus (2004 model) crashing. The same parameters were utilized for 40 km/h, 48 km/h, 64 km/h, 72 km/h velocities of the vehicle, and the results obtained in from Finite Element Analysis (FEA) are in good agreement, as presented in [46]. Hence, it is proved that the structural parameters (lumped parameters) are constant irrespective of the velocities of the vehicle.

The present work is based on the optimized lumped parameters of the vehicle with an initial velocity of 35 km/h as per the experimental result available in [4, 44]. The same parameters have also been utilized for 45, 65, and 85 km/h

velocities due to the fact that the structural parameters are constant irrespective of velocities of the vehicle.

Hence, the dynamic simulation is extended from low-speed to high-speed impact velocities, i.e., from 35 km/h to 85 km/h and is presented in next section.

Results and Discussion

There are various standards in crash test phenomena such as Federal Motor Vehicle Safety Standards (FMVSS) 208-occupant crash protection, New Car Assessment Programme (NCAP), and Insurance Institute of Highway Safety (IIHS). These standards are mostly based on the following performance criteria [47].

- Vehicle’s deceleration pulse
- Occupant peak deceleration
- Passenger compartment intrusion (dynamic crush) or structural deformation
- Head Injury Criteria (HIC)
- Occupant chest deceleration and deformation
- Vehicle Crash Severity Index (VCSI)
- Overall Severity Index (OSI)
- Specific absorbed energy

In the current research, dynamic crush (deformation) and deceleration pulse are used as performance attributes, because, many of the criteria mentioned above depend on these outputs. The safe limit and vehicle crash severity index is also proportional to the deformation and deceleration, respectively. The results can be categorized as one-DoF, and

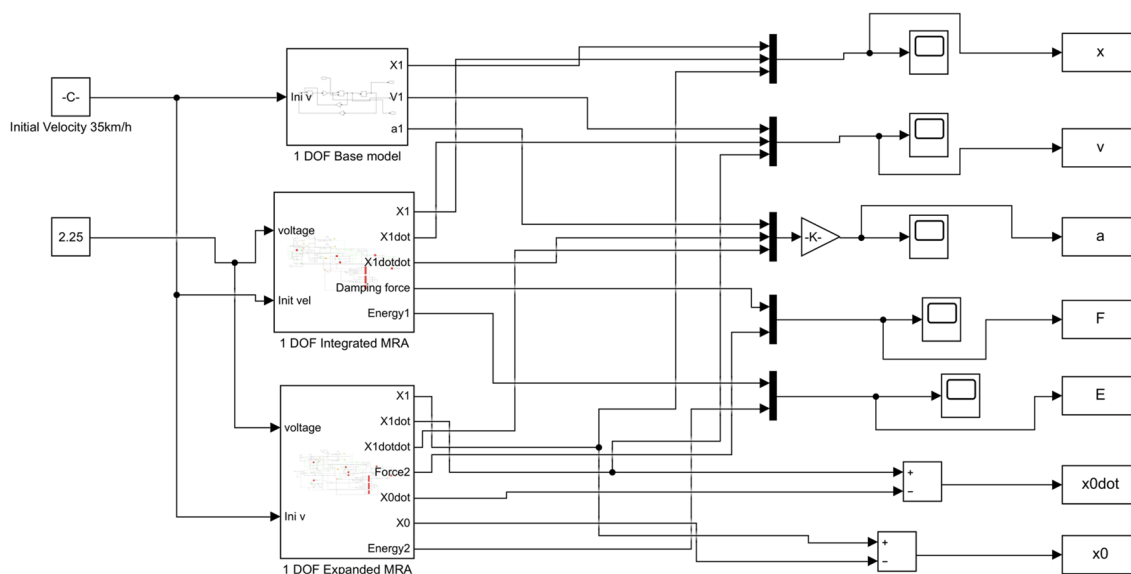


Fig. 6 The Simulink model for one-DoF crash energy absorption system

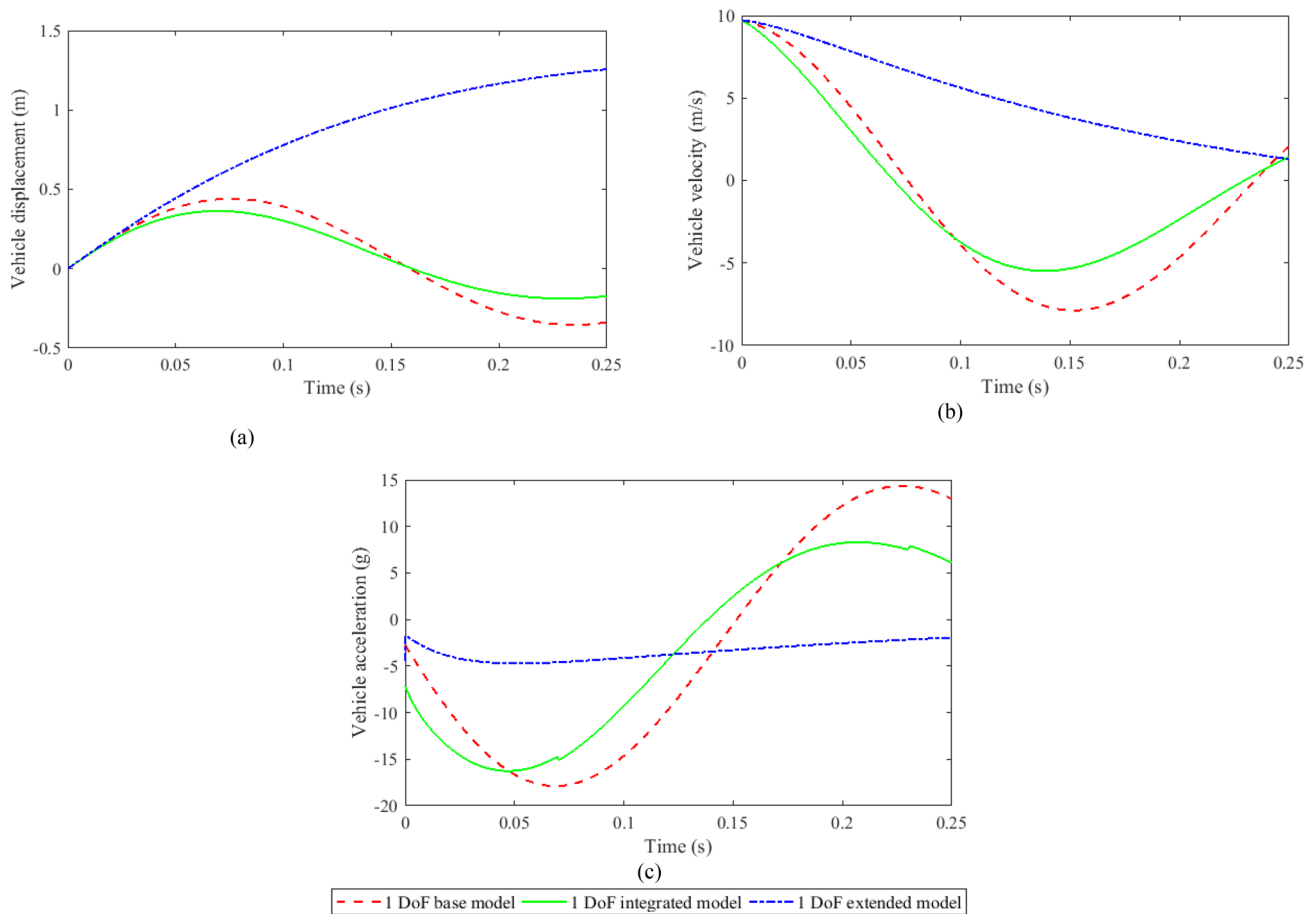


Fig. 7 One-DoF system kinematic response for two different configurations of MRA with a base model at 2.25 V and 35 km/h. **a** Vehicle displacement vs time. **b** Vehicle velocity vs time. **c** Vehicle acceleration vs time

two-DoF crash absorption systems, and also the behavior of MRA has been captured in each case, as explained in successive sub-sections.

One-DoF Crash Absorption System

A one-DoF system has been developed as the Kelvin–Voigt model, and the dynamic equation is derived to find acceleration, velocity, and displacement of the system. Equation (8) is a linear homogeneous second-order ordinary differential equation with constant coefficients, and this is considered as an underdamped free vibration system. The solution of this equation gives the exponentially decaying displacement as per time. Two configurations are proposed, such as integrated and extended models as per the position of MRAs. These MRAs exhibit non-linear hysteresis behavior and are modeled in SIMULINK environment with displacement, external voltage as inputs, and damping force as output, as shown in Fig. 6. The damping force developed by MRA

during collision maintains the vehicle’s kinematic response within the safe limit.

Numerical simulation for a frontal collision of the vehicle has been performed in this work to obtain the vehicle kinematic responses. The vehicle is collided with a fixed barrier at 35 km/h without MRAs and then with two configurations of proposed systems equipped with MRAs for constant voltage 2.25 V. The vehicle experiences a very high dynamic crush of 0.441 m within a short period, i.e., 0.075 s as shown in Fig. 7a, and these results are closer to experimental results of a maximum crush of 0.52 m at 0.076 s. After placing MRAs in integrated mode, the maximum dynamic crush (deformation) and time of crush of the vehicle are 0.411 m at 0.073 s, respectively. The velocity of the vehicle is reducing from 35 to 0 km/h within a short period of almost 0.25 s for the base and proposed models. The integrated model exhibits more reduction in velocity at the time of maximum crush compared with base and extended models, as shown in Fig. 7b. The acceleration vs time response is shown in Fig. 7c, and it depicts that the integrated model gives a better response than the base model.

The base and proposed models of one DoF are also tested with various velocities of the vehicle in an incremental pattern ranging from 35 to 85 km/h, and the responses such as maximum displacement, maximum deceleration of the vehicle gets increased and shown in Table 7.

The integrated model has reduced the dynamic crush and maximum deceleration by 17.47% and 9.03%, respectively, when compared with a collision of the base model at 35 km/h. The reduction percentage is almost similar for velocity ranging from 35 to 85 km/h.

The weighted product method has been adopted in this work due to its popularity in multi-criteria decision analysis with dimensionless capability (independent of the unit of measure) [48]. The present decision-making process involves displacement and deceleration as criteria, and various other models proposed as alternatives. The weighted score as mentioned in (16) has been used as a performance attribute to select the optimal model with minimization as criterion. A weighted normalized matrix has been developed by considering weights as 0.6 and 0.4 for displacement and deceleration, respectively, for four velocities as shown in Table 8. Displacement should be as minimum as possible otherwise there would be more damages during collision and hence higher weightage is considered for displacement compared to deceleration. The results confirmed that the integrated model gives better weighted score amongst all other models. Thus, a vehicle with an integrated MRA would be the best option compared with the extended case. Hence, the behavior of MRA is estimated only for the integrated case as presented below.

The weighted score is

$$P(X_I/X_J) = \prod_{k=1}^n (x_{Ik}/x_{Jk})^{w_j}, \text{ for } I, J = 1, 2, 3, \dots, m, \quad (16)$$

where $X_{min} = X_i$ for minimization problem.

The damping force developed in the integrated model is shown in Fig. 8a, and it depicts that the peak damping force is initially high, then exponentially decaying with respect to time and finally becomes zero. When a vehicle hits a stationary barrier with the high velocity, it experiences a high crushing force and deceleration within a short period. To achieve a reduction in the dynamic crush with an acceptable deceleration period, two numbers of MRA are used in an integrated model and operated at controllable voltages as per the impact force experienced by the system.

In the force–displacement response shown in Fig. 8b, the damping force varies between negative and positive displacements, which resembles the involute pattern because the displacement response of the system is exponentially decaying. The large radial curve is formed initially for high displacement and keeps on reducing step by step through a decrease in the displacement of the response and finally becomes zero. A similar pattern is observed with damping force versus displacement response at various external voltages. The damping force of the MRA varies proportionately with the piston velocity for various voltages ranging from 0 to 2.25 V and creates an asymmetric hysteresis loop (Fig. 8c) because of high impact velocity is experienced by MRA.

MRA behavior is also investigated for different initial velocities of the vehicle operated at a constant voltage of 2.25 V. The damping force generated is initially high when the vehicle impacts the fixed barrier and decaying exponentially as per the time. Moreover, it is also proportionally varying with velocity, as shown in Fig. 9a. The force–displacement response, as shown in Fig. 9b interprets that, the damping force generated is being adjusted according to dynamic crush or amplitude. It shows an involute profile starts with certain damping force and reaches a maximum

Table 7 Maximum displacement and maximum deceleration at constant voltage 2.25 V for various velocities of the vehicle with one-DOF models

Entity/model	Maximum displacement (m)				Maximum deceleration (g)			
	35	45	65	85	35	45	65	85
Initial velocity, km/h								
Base model	0.4407	0.5666	0.8185	1.0703	17.8851	22.9952	33.2153	43.4354
Integrated model	0.3637	0.4665	0.6722	0.8779	16.269	20.9468	30.3027	39.6588
Extended model	1.2566	1.6031	2.2962	2.9893	4.7084	6.1078	8.907	11.7063

Table 8 Weighted product method for selection of the best model amongst the one-DoF models proposed

Criteria / Alternatives	Maximum displacement				Maximum deceleration				Weighted score
	Weighted-Normalized decision matrix with $w=0.15$				Weighted-Normalized decision matrix with $w=0.1$				
Base model	0.9716	0.9713	0.9709	0.9707	0.8751	0.8758	0.8767	0.8771	0.5241
Integrated model	1.0000	1.0000	1.0000	1.0000	0.8834	0.8840	0.8848	0.8851	0.6116
Extended model	0.8303	0.8310	0.8317	0.8321	1.0000	1.0000	1.0000	1.0000	0.4775

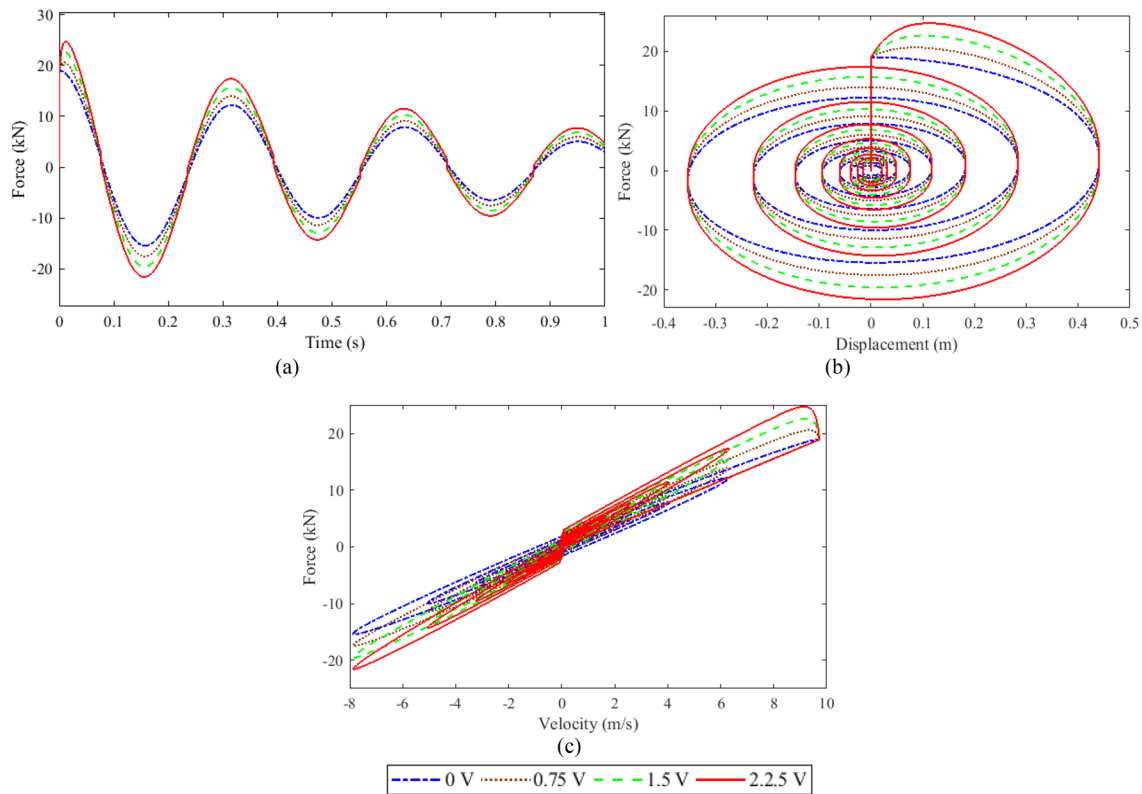


Fig. 8 Characteristic plots of MRA in one-DoF integrated model for different voltages at constant velocity 35 km/h. **a** Force vs time. **b** Force vs displacement. **c** Force vs velocity

value of 59 kN at the positive displacement of 0.2 m, which also oscillates between negative and positive displacements. Simultaneously, the force decreases step by step in an involute pattern based on variation in the amplitude of the response. The damping force varies proportionately with the velocity of the vehicle and creates an asymmetrical hysteresis pattern, as shown in Fig. 9c.

Two-DoF Crash Absorption System

In this study, four proposed models are numerically studied and compared with the two-DoF base model in terms of the kinematic responses of frontal parts of the vehicle and occupant's cabin. The diagrammatic representation of the mathematical equation in Simulink is shown in Fig. 10. The output parameters such as displacement, velocity, and acceleration responses of both occupant's cabin and frontal parts of the vehicle for a constant speed of 35 km/h at the voltage of 2.25 V applied externally to the MRA are shown in Fig. 10. When using two-DoF base model, the maximum dynamic crush of occupant's cabin is 0.5334 m, which is also matching closely with a real test result of 0.52 m.

Amongst the proposed models, the Integrated models, which are developed by incorporating MRA in front of lumped masses M_1 and M_2 , are giving better maximum dynamic crush of 0.472 m and 0.475 m, respectively (Fig. 11a) for occupant's cabin. The maximum dynamic crush of the vehicle is 0.342 m for the base model, and for two integrated models, the values are 0.276 m, 0.348 m, respectively, which are less than the response of the base model. The velocity–time reactions of both the vehicle and occupant's cabin are shown in Fig. 11b, which depicts that all models are starting with the same initial velocity of 9.772 m/s (35 km/h) and are reaching zero within a short period of 0.125 s approximately except extended models. The integrated M_1 model exhibits more reduction of velocity at the time of crush for both vehicle and occupant's cabin. The acceleration response is shown in Fig. 11c for both the occupant's cabin and the vehicle. This proves that the extended models exhibit better results than integrated models, but they are experiencing a high displacement response. Hence, it can be observed that the integrated models provide a good agreement of results in terms of displacement, velocity, and acceleration for both vehicle and occupant's cabin compared with the base model.

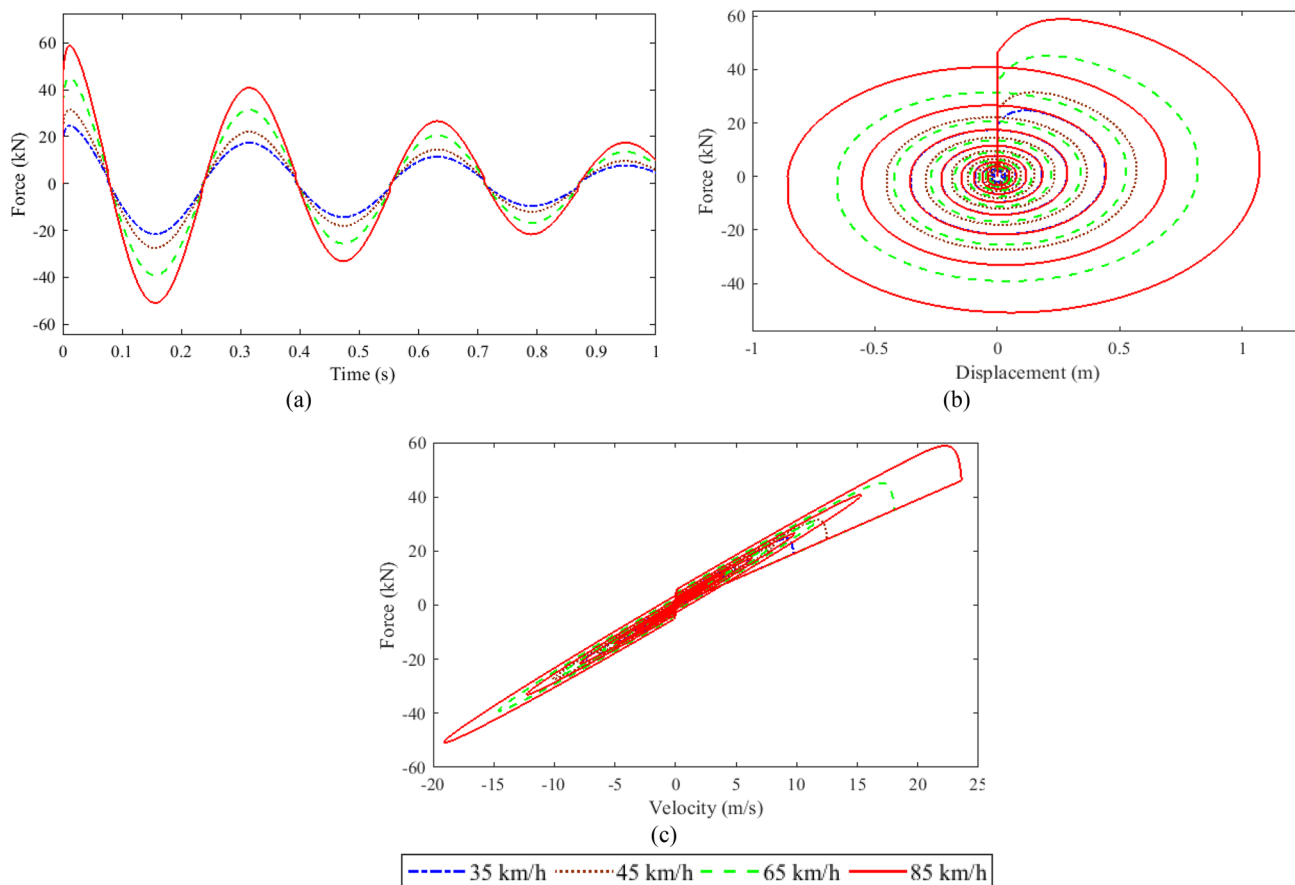


Fig. 9 Characteristic plot of MRA in one-DoF integrated model for different velocities at constant voltage 2.25 V. **a** Force vs time. **b** Force vs displacement. **c** Force vs velocity

The maximum displacement, maximum deceleration for both the vehicle and occupant’s cabin are plotted for various velocities ranging from 35 to 85 km/h at constant voltage 2.25 V (Fig. 12) to evaluate the behavior of the proposed models for higher velocities. The peak displacement of the vehicle and the occupant’s cabin for all models is increased due to an increase in initial velocity, i.e., from 35 to 85 km/h, which is shown in Fig. 12a. It is observed that two integrated models have less peak displacement of occupant’s cabin than the other models, including the base model. Whereas, the vehicle’s peak displacement is less for all models except for the extended M_1 model. The deceleration of both the vehicle and occupant’s cabin is also proportional to the initial velocity. Two integrated models exhibit a lower deceleration response when compared with extended models, but the response is still higher than the base model, as shown in Fig. 12b. Even though the deceleration of occupant’s cabin is more compared with the base model, it is within the permissible limit for human safety. The deceleration response of the vehicle for integrated M_2 almost coincides with the base model. An extended M_1 model exhibits less deceleration response than other models due to an add-on MRAs in

front of mass M_1 . These MRAs absorb most of the energy experienced by frontal parts of the vehicle at high impact during the primary stage of collision.

The maximum displacement and the maximum deceleration of the occupant’s cabin for various velocities are calculated and tabulated in Table 9. The weighted product method with the weighted score mentioned in (16), as a performance index, has been used to obtain the optimal one amongst the proposed two-DoF models. The integrated models are selected as the best models amongst all as per the weighted normalized decision matrix as presented in Table 10.

The MRA behavior is obtained only for the integrated models because they exhibit appropriate displacement of occupant’s cabin and vehicle within the permissible deceleration compared to extended MRA models.

The damping force generated by MRA is initially high for the integrated M_1 model compared with the integrated M_2 model, as shown in Fig. 13a.

The reason is when MRA is placed in front of the vehicle lumped mass M_1 , there is a high collision force experienced by MRA, and a large damping force is produced to overcome it. Thus, a large damping force is generated

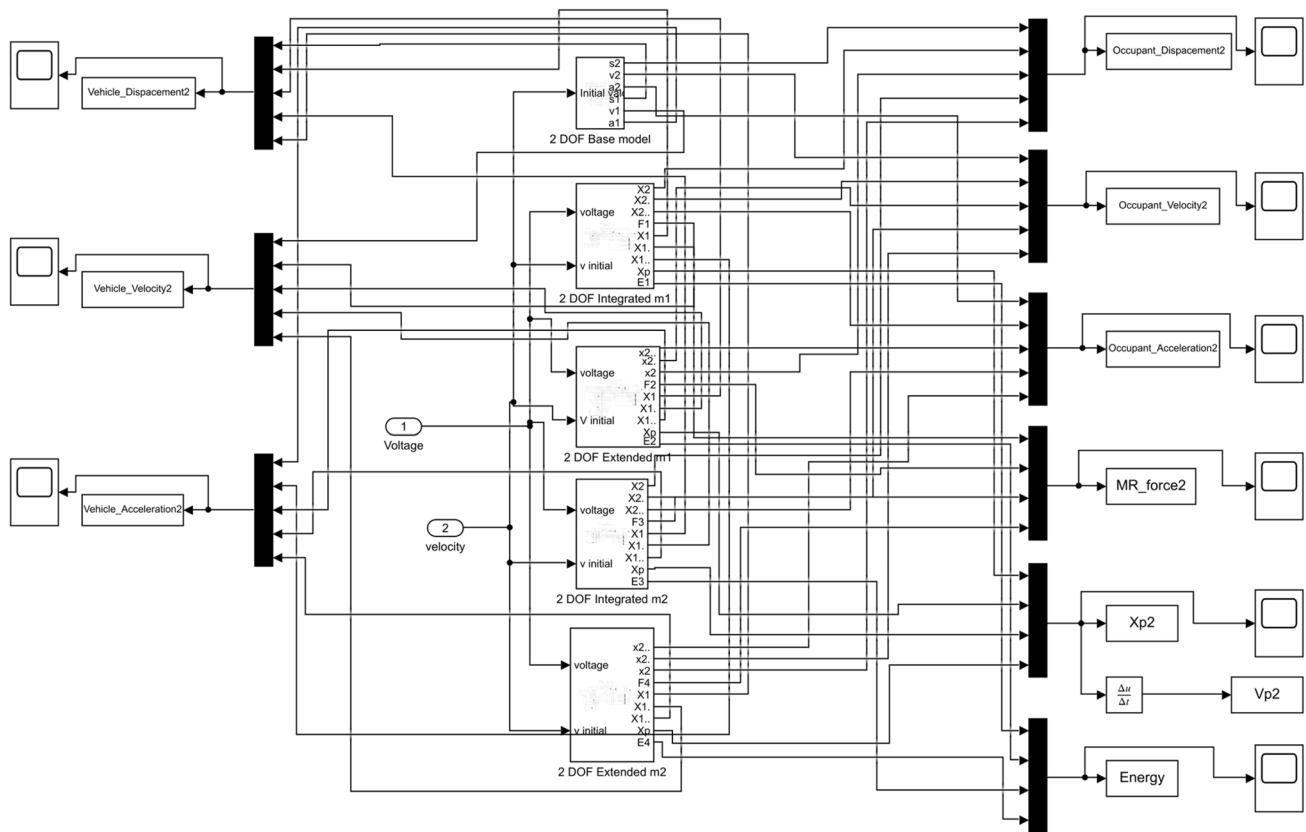


Fig. 10 The Simulink model for two-DoF crash energy absorption system

for the integrated M_1 model, follows a non-linear pattern by an increase in displacement, and finally reaches zero. Whereas the integrated M_2 model experiences a secondary impact force after crushing the frontal parts of the vehicle, thus, MRA produces initially low damping force compared to the previous model. The damping force of integrated M_1 is high at the initiation of the collision, and then it increases non-linearly up to a peak of 20.14 kN, and finally reduces linearly along with an increase in displacement. Whereas the integrated M_2 model initially produces a low damping force of 6.63 kN because of a low range of displacement, as shown in Fig. 13b. The damping force vs velocity response, as shown in Fig. 13c, describes the non-linear hysteresis behavior of the integrated M_2 model and abnormal behavior of the integrated M_1 model.

The energy absorbed by the MRA is calculated according to (17) based on various initial velocities of the vehicle and presented in Table 11. Also, it can be observed that the one-DoF integrated M_1 model absorbs more energy because it experiences high damping force during collision. Whereas, the two-DoF model integrated with M_1 absorbs more energy during collision as it is in the front side of the vehicle.

The energy absorbed by MRA is

$$E_{MR} = \int F \cdot d(x_{rel}), \quad (17)$$

where, F is damping force generated by MRA, and x_{rel} is the relative displacement of the MRA piston.

The maximum displacement of MRA against various velocities and voltages has been studied. The simulation data are presented in Table 12.

The following inferences have been drawn from Table 12.

- In the case of 1-DoF model, the maximum stroke of MRA increases from 0.4407 to 1.0702 m for velocities ranging from 35 to 85 km/h irrespective of the voltage applied.
- The maximum displacement of MRA varies from 0.2762 to 0.7080 m and from 0.1280 to 0.3580 m for 2-DoF integrated model with M_1 and M_2 , respectively. It is indirectly proportional to the voltage and directly proportional to the velocity of the vehicle.
- Thus, the maximum stroke varies with the configuration, impact velocity, voltage, and DoF of the model.

It is also revealed that by increasing the DoF of the dynamic model, there is a reduction of maximum stroke of

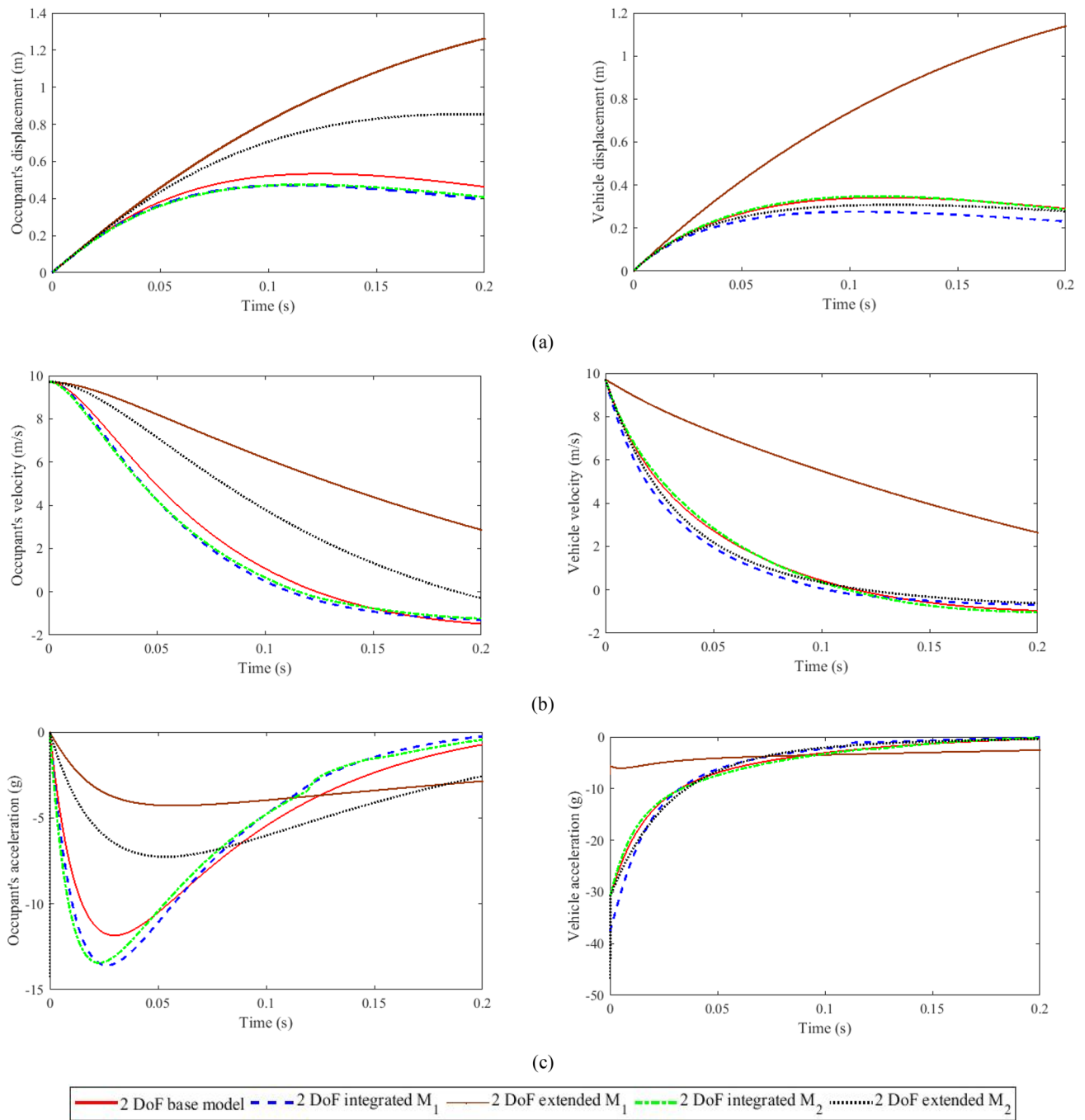


Fig. 11 Crash kinematics of frontal parts of vehicle and occupant's cabin for various models with constant voltage 2.25 V applied to MRA at 35 km/h. **a** Occupant's and vehicle displacement vs time. **b**

Occupant's and vehicle velocity vs time. **c** Occupant's and vehicle acceleration vs time

MRA. In this simulation, the maximum stroke of MRA for 1 DoF model with high impact velocity, i.e., at 85 km/h is reaching 1 m and it is not feasible. Hence, it has been suggested to go for higher DoF models for higher impact velocities. The length of the front overhang of the passenger cars lies between 0.8 and 1.2 m [49]. Hence, this limited space

is considered for the proposed model. Future investigations will be focused on size optimization while increasing the DoF of the model considering the availability of limited space.

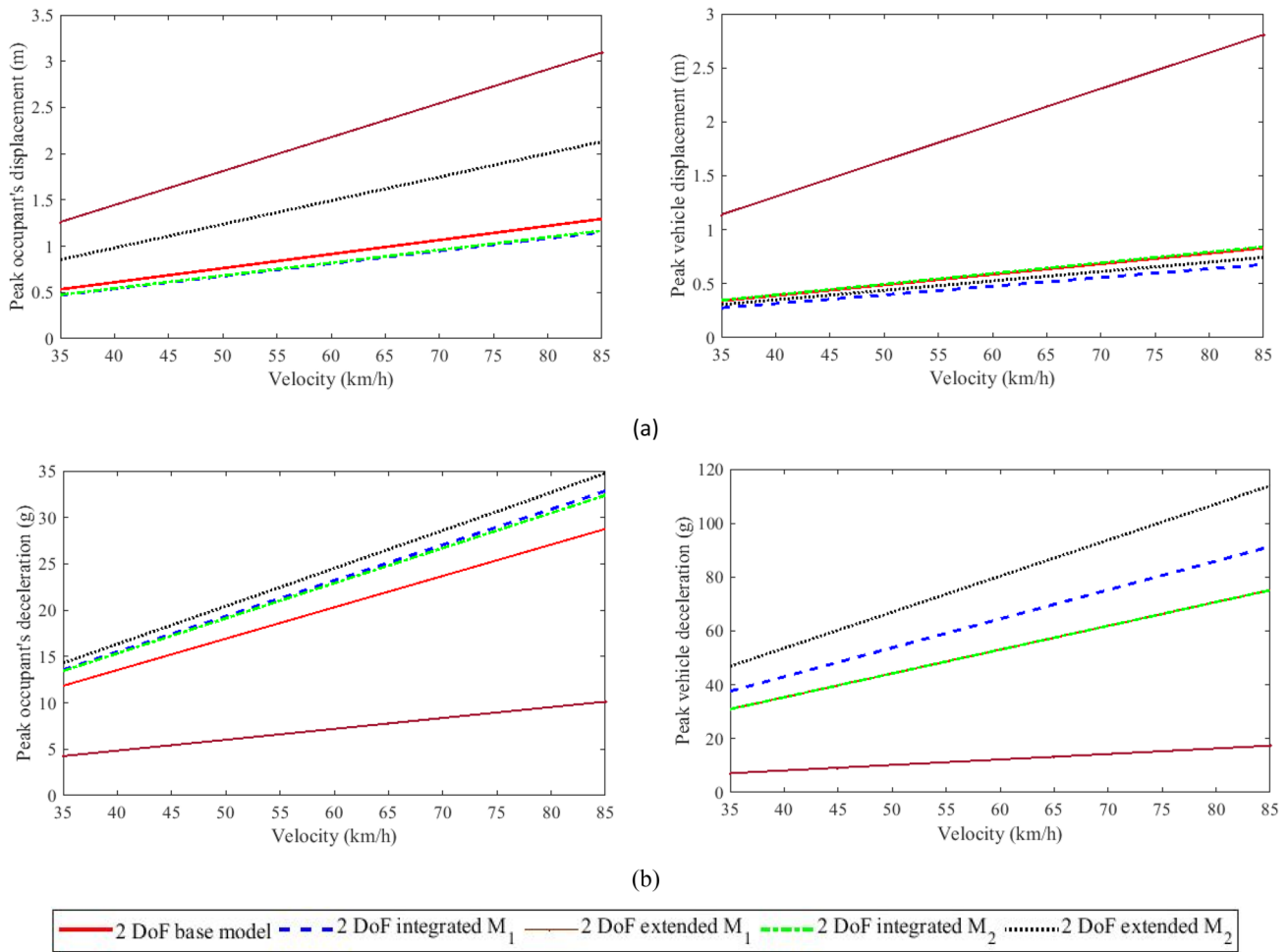


Fig. 12 Crash pulse for different models with various velocities at constant voltage 2.25 V. **a** Initial velocity vs Occupant’s and vehicle displacement. **b** Initial velocity vs Occupant’s and vehicle deceleration

Table 9 Maximum displacement and maximum deceleration at constant voltage 2.25 V for various velocities of the vehicle with two-DoF models

Entity/Model	Maximum displacement (m)				Maximum deceleration (g)				
	Initial Velocity, km/h	35	45	65	85	35	45	65	85
Two-DoF Base model		0.5334	0.6858	0.9906	1.2955	11.8476	15.2326	22.0026	28.7727
Two-DoF integrated M1		0.4718	0.6079	0.8800	1.1522	13.5796	17.429	25.1279	32.8267
Two-DoF extended M1		1.2614	1.6282	2.3617	3.0952	4.2584	5.4326	7.7811	10.1295
Two-DoF integrated M2		0.4752	0.6135	0.8902	1.1669	13.4408	17.2303	24.8098	32.3898
Two-DoF extended M2		0.8542	1.1093	1.6198	2.1305	14.3038	18.3907	26.5643	34.7379

The design of the proposed collision energy absorption system integrated with MRA has been validated based on the experimental results available in [4] and [44].

The development of dynamic mathematical models itself is complicated due to the consideration of non-linearity in the system. Hence, the optimized results obtained based on the current simulation work would be tested further

experimentally with a prototype that is being fabricated, and the results will be presented in future communications.

The following are the technical significance of the proposed work.

Table 10 Weighted product method for selection of the best model amongst the two-DoF models proposed

Criteria / Alternatives	Maximum displacement				Maximum deceleration				Weighted score
	Weighted-Normalized decision matrix with $w=0.15$				Weighted-Normalized decision matrix with $w=0.1$				
Two-DoF base model	0.9818	0.9821	0.9824	0.9826	0.9027	0.9020	0.9013	0.9009	0.6153
Two-DoF integrated M1	1.0000	1.0000	1.0000	1.0000	0.8905	0.8900	0.8894	0.8891	0.6267
Two-DoF extended M1	0.8629	0.8626	0.8624	0.8622	1.0000	1.0000	1.0000	1.0000	0.5534
Two-DoF integrated M2	0.9989	0.9986	0.9983	0.9981	0.8914	0.8910	0.8905	0.8903	0.6259
Two-DoF extended M2	0.9148	0.9137	0.9125	0.9119	0.8859	0.8852	0.8845	0.8841	0.4265

Table 11 Maximum energy absorbed by MRA at constant voltage 2.25 V for both one- and two-DOF integrated models

Model /Initial velocity	Maximum energy absorbed by MRA (kJ)		
	One DoF integrated	Two-DoF integrated M1	Two-DoF integrated M2
35 km/h	3.9230	2.0150	1.8240
45 km/h	6.5650	3.2810	2.9310
65 km/h	13.8760	6.7320	5.9260
85 km/h	23.8900	11.4110	9.9630

- The proposed models can be utilized especially in EVs to reduce the risk of passengers during frontal collision due to the absence of an engine cabin.
- The models consume low power and generate high damping force during collision by altering the voltage supplied to MRA.
- Technically contribute to further development of multi-DoF collision energy absorption systems utilizing the smart nature of MRA.
- This work contributes in development of dynamic mathematical models and their simulation which would to avoid an expensive experimental setup.

The importance of the present work is to ensure MR technology's capability in the context of impact energy absorption, especially in a vehicle crash. In this work, the MRA, which is semi-active in nature and responds within a range of milliseconds with high damping force, played an appropriate role in absorbing the collision energy. The proposed models are also useful in frontal crash mitigation of EVs by supplying the required power to MRA as per the severity of impact.

Conclusion

An attempt has been made to propose a new design of a crash energy absorption system by incorporating Magneto-Rheological Absorber (MRA). The system's performance was studied considering various MRA positions in the lumped parameter model of one and two degrees of freedom. The MRA has been modeled based on the modified Bouc–Wen non-linear hysteresis model. Numerical simulation was performed with available parameters in SIMULINK to validate the damper characteristics. The dynamic equations of proposed models that are series and parallel configurations of MRAs with the vehicle structure were derived using Newton's second law of motion. The numerical simulation parameters, such as stiffness, damping coefficient, and masses, were considered from the literature that had been validated using real-time crash tests.

The results are categorized as one- and two-DoF models. In the simulation of one-DoF model, the MRA model exhibits better crash pulse characteristics in terms of the maximum dynamic crush and maximum deceleration. These characteristics were reduced by 17.47% and 9.04%, respectively, when compared with the base model for a speed of 35 km/h and a constant voltage of 2.25 V. In the two-DoF model, an attempt was made considering the frontal parts of the vehicle and occupants cabin as two different masses. The integrated MRA models show proper crash pulse characteristics amongst all the four models proposed here. The study continued for various velocities ranging from 35 to 85 km/h for capturing the kinematics of the vehicle. The best integrated models have been selected based on the weighted product method for both the one-DoF and two-DoF models proposed. Finally, the investigation on the characteristics of MRA has been performed for selected models of one- and two-DoF systems to reveal the behavior of MRA, especially in high-velocity impact situations. Hence, the collision energy absorption system with add-on MRAs behaves as a semi-active system. It is efficient during various high-speed impacts and can be implemented practically.

The future scope is to develop a control scheme for feasible collision energy absorption models to adjust the

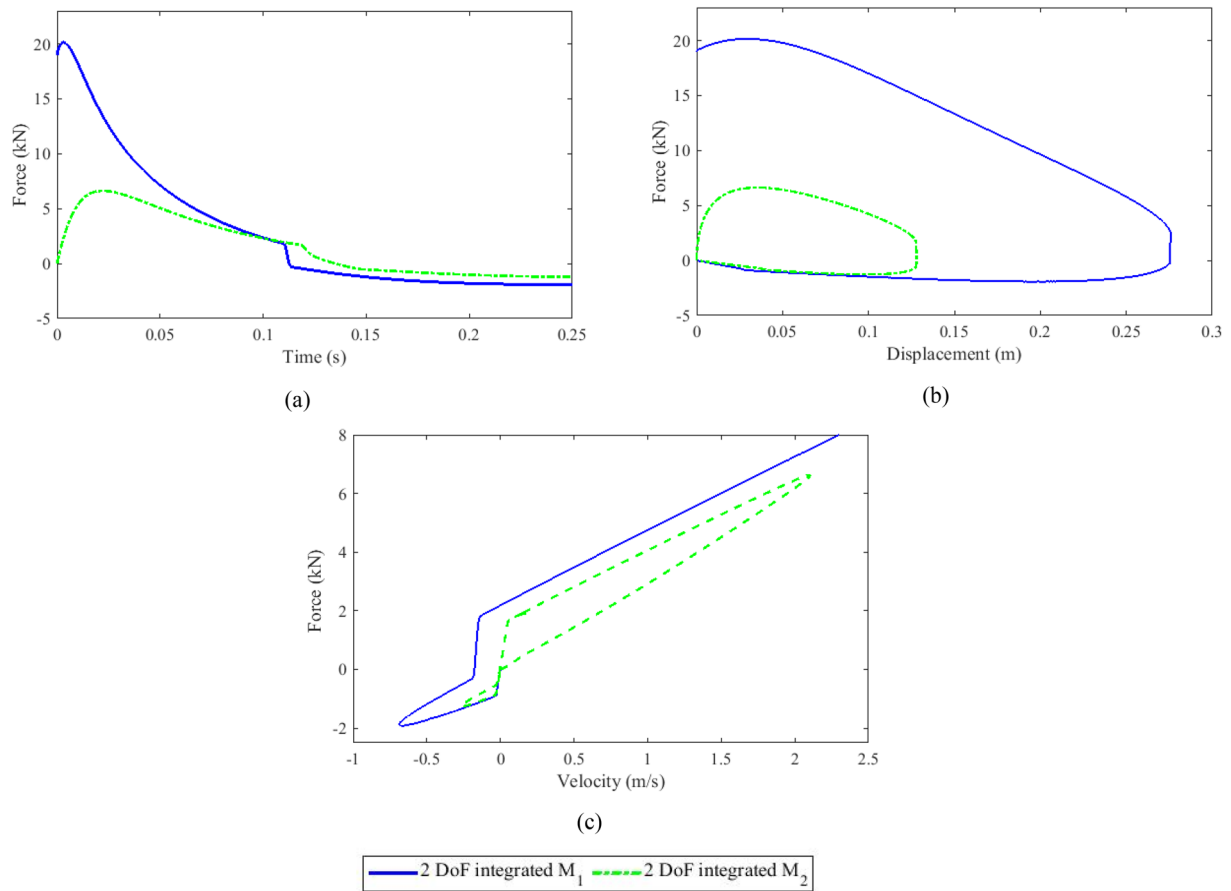


Fig. 13 Characteristic plots for MRA in two-DoF integrated MRA crash system for 35 km/h and 2.25 V. **a** Force vs. time. **b** Displacement vs. force. **c** Velocity vs. force

Table 12 Maximum displacement (Stroke) of MRA during crash (m)

Voltage/ velocity	1-DoF integrated model				2-DoF integrated model with M_1				2-DoF integrated model with M_2			
	0 V	0.75 V	1.5 V	2.25 V	0 V	0.75 V	1.5 V	2.25 V	0 V	0.75 V	1.5 V	2.25 V
35 km/h	0.4407	0.4407	0.4407	0.4407	0.2912	0.2860	0.2810	0.2762	0.1468	0.1401	0.1338	0.1280
45 km/h	0.5666	0.5666	0.5666	0.5666	0.3746	0.3683	0.3623	0.3566	0.1890	0.1814	0.1743	0.1676
65 km/h	0.8184	0.8184	0.8184	0.8184	0.5413	0.5330	0.5250	0.5174	0.2735	0.2641	0.2553	0.2469
85 km/h	1.0702	1.0702	1.0702	1.0702	0.7080	0.6976	0.6877	0.6782	0.3580	0.3468	0.3362	0.3263

magnetic field strength in accordance with the impact force experienced by the vehicle during the collision, which would make the entire system intelligent. For this work, the required parameters of the MRA model were directly considered from the available literature. The possibility to optimize these parameters with a suitable optimization algorithm as per the collision severity will be investigated further.

Declarations

Conflict of interest The authors declare that they have no conflict of interest.

References

1. Road safety and injury prevention. In: WHO India. http://www.searo.who.int/india/topics/road_safety_and_injury_prevention/en/.

2. Livesey WA, Robinson A (2000) The repair of vehicle bodies. Elsevier
3. Lim JM (2017) Lumped mass-spring model construction for crash analysis using full frontal impact test data. *Int J Automot Technol* 18:463–472
4. Pawlus W, Karimi HR, Robbersmyr KG (2011) Development of lumped-parameter mathematical models for a vehicle localized impact. *J Mech Sci Technol* 25:1737–1747
5. Kamal MM (2010) Analysis and Simulation of Vehicle to Barrier Impact. *SAE Tech Pap Ser* 1:1498–1503
6. Rabinow J (1948) The magnetic fluid clutch. *Trans Am Inst Electr Eng* 67:1308–1315
7. Ashtiani M, Hashemabadi SH, Ghaffari A (2015) A review on the magnetorheological fluid preparation and stabilization. *J Magn Magn Mater* 374:716–730
8. Ahamed R, Choi S (2018) A state of art on magneto-rheological materials and their potential applications. *J of Intelligent Mater Syst Struct* 29:1–45
9. Liu X, Gao X, Yu H, Ye D (2015) Dynamic performance of different metal foam magnetorheological fluid materials. *IEEE Trans Magn* 51:1–5
10. Liu X, Gao X, Li F, Yu H, Ye D (2015) Shear Performance of a Metal Foam. *IEEE Trans Magn* 51:1–7
11. Yuan X, Tian T, Ling H, Qiu T, He H (2019) A review on structural development of magnetorheological fluid damper. *Shock Vib* 2019:1–33
12. Rahman M, Ong ZC, Julai S, Ferdaus MM, Ahamed R (2017) A review of advances in magnetorheological dampers: their design optimization and applications. *J Zhejiang Univ A* 18:991–1010
13. Spencer BFJ, Dyke SJ, Sain MK, Carlson JD (1996) Phenomenological Model of a Magnetorheological Damper. *ASCE J Eng Mech* 1–23
14. Jamadar M e. H, Desai RM, Saini RST, Kumar H, Joladarashi S (2020) Dynamic Analysis of a Quarter Car Model with Semi-Active Seat Suspension Using a Novel Model for Magneto-Rheological (MR) Damper. *J Vib Eng Technol*. <https://doi.org/https://doi.org/10.1007/s42417-020-00218-1>
15. Spencer BF, Yang G, Carlson JD, Sain MK (1998) Smart dampers for seismic protection of structures : a full-scale study. *Proc 2nd World Conf Struct Control* 1:1–10
16. Lv H, Zhang S, Sun Q, Chen R, Zhang WJ (2020) The Dynamic Models, Control Strategies and Applications for Magnetorheological Damping Systems: A Systematic Review. *J Vib Eng Technol*. <https://doi.org/https://doi.org/10.1007/s42417-020-00215-4>
17. Ma Y, Xie S, Zhang X, Luo Y (2013) Hybrid modeling approach for vehicle frame coupled with nonlinear dampers. *Commun Nonlinear Sci Numer Simul* 18:1079–1094
18. Hu G, Yi F, Liu H, Zeng L (2020) Performance analysis of a novel magnetorheological damper with displacement self-sensing and energy harvesting capability. *J Vib Eng Technol*. <https://doi.org/10.1007/s42417-020-00212-7>
19. Cheng M, Chen ZB, Xing JW (2018) Design, analysis, and experimental evaluation of a magnetorheological damper with meandering magnetic circuit. *IEEE Trans Magn* 54:1–10
20. Ahmadian M, Norris JA (2008) Experimental analysis of magnetorheological dampers when subjected to impact and shock loading. *Commun Nonlinear Sci Numer Simul* 13:1978–1985
21. Bin Pokaad AZ, Nasir MZM, Ubaidillah (2011) Simulation and experimental studies on the behavior of a magnetorheological damper under impact loading. 2011 4th Int Conf Mechatronics Integr Eng Ind Soc Dev ICOM'11 - Conf Proc 2:164–187
22. bin Pokaad AZ, Hudha K, bin Said MR, (2013) Usage of magnetorheological damper in active front bumper system for frontal impact protection. *Appl Mech Mater* 315:40–44
23. Dong X, Guan Z (2011) Human simulated sliding mode control for vehicle collision absorbing system based on magneto-rheological absorber. *Proc 2nd Int Conf Intell Control Inf Process ICICIP* 2011 2:956–960
24. Imthiyaz Ahamed T, Sundarrajan R, Prasaath GT, Raviraj V (2014) Implementation of Magneto-rheological dampers in bumpers of Automobiles for reducing impacts during accidents. *Procedia Eng* 97:1220–1226
25. Bai X, Hu W, Wereley NM (2013) Magnetorheological damper utilizing an inner bypass for ground vehicle suspensions. *IEEE Trans Magn* 49:3422–3425
26. Sun L, Li W, Guo S, Chen W (2013) A magnetorheological-elastomer-based energy absorption device for car crash protection. *Int J Veh Des* 63:223–240
27. Woo D, Choi SB, Choi YT, Wereley NM (2007) Frontal crash mitigation using MR impact damper for controllable bumper. *J Intell Mater Syst Struct* 18:1211–1215
28. Wang J, Li Y (2006) Dynamic simulation and test verification of MR shock absorber under impact load. *J Intell Mater Syst Struct* 17:309–314
29. Arsava KS, Kim Y (2015) Modeling of magnetorheological dampers under various impact loads. *Shock Vib* 2015:1–20
30. Elmarakbi AM, Zu JW (2004) Dynamic modeling and analysis of vehicle smart structures for frontal collision improvement. *Int J Automot Technol* 5:247–255
31. Jawad S (2010) Smart structures for frontal collision mitigation. *SAE Tech Pap Ser*. <https://doi.org/10.4271/2002-01-0247>
32. Fadlallah SO, Al RNZ, Al SAM, Chenhui K, Goher KM (2017) Transient dynamic impact suppression of a Baja chassis using frontal and rear shock absorbers. *Int J Crashworthiness* 22:676–688
33. Elmarakbi AM, Zu JW (2006) Crash analysis and modeling of two vehicles in frontal collisions using two types of smart front-end structures: An analytical approach using IHBM. *Int J Crashworthiness* 11:467–483
34. Cao LB, Wang HB, Wu J, Chen HQ (2012) Study on a pneumatic automatic-extendable crash energy absorption system. *Adv Mater Res* 455–456:1509–1514
35. Jain S, Sreekumar M (2016) The Preliminary Design of a Collision Energy Absorption System. 6th Int 27th All India Manuf Technol Des Res Conf Pune, Maharashtra, INDIA 779–782
36. Feng H, Lu X, Qiao Y, Chen X (2019) Crashworthiness analysis of electric vehicle with energy-absorbing battery modules. *J Eng Mater Technol* doi 10(1115/1):4035498
37. Wang DH, Liao WH (2011) Magnetorheological fluid dampers: a review of parametric modelling. *Smart Mater Struct* 20:1–34
38. Pan W, Yan Z, Lou J, Zhu S (2018) Research on MRD parametric model based on magic formula. *Shock Vib* 2018:10
39. Song X, Engineer P, Ahmadian M, Southward SC (2005) Modeling magnetorheological dampers with application of nonparametric approach. *J Intell Mater Syst Struct* 16:421–432
40. Duchanoy CA, Moreno-armendáriz MA, Moreno-torres JC (2019) A deep neural network based model for a kind of magnetorheological dampers. *MDPI sensors* 19:1–18
41. Eshkabilov SL (2016) Modeling and simulation of non-linear and hysteresis behavior of magneto-rheological dampers in the example of quarter-car model by using MATLAB® / Simulink®. *Commun Control Sci Eng* 4:12–29
42. Jiang K, Wen J (2020) Identification of nonlinear hysteretic systems using sequence model-based optimization. *Struct Control Heal Monit* 27:1–24
43. Farahmand B, Veladi H, Talatahari S, Raeesi F (2020) Optimal design of magnetorheological damper based on tuning bouc-wen model parameters using hybrid algorithms. *KSCE J Civ Eng* 24:867–878
44. Munyazikwiye BB, Karimi HR, Robbersmyr KG (2013) Mathematical modeling and parameters estimation of car crash using

- eigensystem realization algorithm and curve-fitting approaches. *Math Probl Eng* 2013:1–13
45. Pawlus W, Karimi HR, Robbersmyr KG (2014) Investigation of vehicle crash modeling techniques: Theory and application. *Int J Adv Manuf Technol* 70:965–993
 46. B. Muniyazikwiye B, Vysochinskiy D, Khadyko M, G. Robbersmyr K, (2018) Prediction of vehicle crashworthiness parameters using piecewise lumped parameters and finite element models. *Designs* 2:43
 47. El-Rahman Khattab AA (2010) Investigation of an adaptable crash energy management system to enhance vehicle crashworthiness. Concordia University Montreal, Quebec, Canada
 48. Mateo JRSC (2012) Weighted sum method and weighted product method. In: *Multi Criteria Anal. Renew. Energy Ind. Green Energy Technol.* pp 19–22
 49. Jeya Padmanaban (2003) Influences of vehicle size and mass and selected driver factors on odds of driver fatality. *47th Annu Proc Assoc Adv Automot Med* 507–524

Publisher's Note Springer Nature remains neutral with regard to jurisdictional claims in published maps and institutional affiliations.